Uncover Topology by Quantum Quench Dynamics

Wei Sun,[1,2,3] Chang-Rui Yi,[1,2,3] Bao-Zong Wang,[1,2,4,5] Wei-Wei Zhang,[6] Barry C. Sanders,[1,7,8] Xiao-Tian Xu,[1,2,3] Zong-Yao Wang,[1,2,3] Joerg Schmiedmayer,[9] Youjin Deng,[1,2,3] Xiong-Jun Liu,[4,5,*] Shuai Chen,[1,2,3,†] and Jian-Wei Pan[1,2,3,‡]

[1]*Shanghai Branch, National Laboratory for Physical Sciences at Microscale and Department of Modern Physics, University of Science and Technology of China, Shanghai 201315, China*

[2]*Chinese Academy of Sciences Center for Excellence: Quantum Information and Quantum Physics, University of Science and Technology of China, Hefei Anhui 230326, China*

[3]*CAS-Alibaba Lab for Quantum Computation, Shanghai 201315, China*

[4]*International Center for Quantum Materials, School of Physics, Peking University, Beijing 100871, China*

[5]*Collaborative Innovation Center of Quantum Matter, Beijing 100871, China*

[6]*Centre for Engineered Quantum Systems, School of Physics, The University of Sydney, Sydney, New South Wales 2006, Australia*

[7]*Institute for Quantum Science and Technology, University of Calgary, Calgary, Alberta T2N 1N4, Canada*

[8]*Program in Quantum Information Science, Canadian Institute for Advanced Research, Toronto, Ontario M5G 1Z8, Canada*

[9]*Vienna Center for Quantum Science and Technology, Atominstitut, TU Wien, Stadionallee 2, 1020 Vienna, Austria*

(Received 10 May 2018; revised manuscript received 21 August 2018; published 18 December 2018)

Topological quantum states are characterized by nonlocal invariants. We present a new dynamical approach for ultracold-atom systems to uncover their band topology, and we provide solid evidence to demonstrate its experimental advantages. After quenching a two-dimensional (2D) Chern band, realized in an ultracold ^{87}Rb gas from a trivial to a topological parameter regime, we observe an emerging ring structure in the spin dynamics during the unitary evolution, which uniquely corresponds to the Chern number for the postquench band. By extracting 2D bulk topology from the 1D ring pattern, our scheme displays simplicity and is insensitive to perturbations. This insensitivity enables a high-precision determination of the full phase diagram for the system's band topology.

DOI: 10.1103/PhysRevLett.121.250403

Topological quantum matter has been a significant topic of investigation since the celebrated discovery of the quantum Hall effect [1,2]. Unlike symmetry-breaking phases of local order parameters, topological quantum states feature nonlocal topological invariants [3], which usually do not connect directly to local physical observables. Characterizing topological states or phases is often challenging. In solid-state experiments, various characterization strategies have been successfully developed for the discovery of topological insulators [4–7] and semimetals [8,9]. Nevertheless, these strategies do not directly measure topological numbers in some circumstances and do not provide explicit evidence for topological quantum phases, such as Majorana modes in the topological superconductivity [10–13].

A variety of strategies for detecting topology for an ultracold-atom system have also been developed. A one-dimensional (1D) Su-Schrieffer-Heeger model in a 1D superlattice has a band topology that can be determined by measuring the Zak phase [14]. Topology of a 2D Chern insulator, characterized by Chern invariants, can be observed by Hall transport [15,16], by Berry curvature mapping [17], by imaging spin polarization at symmetric Bloch momenta [18–20]. Recently, the quantum quench for topological systems has attracted attention, with the dynamical quantum phase transition [21–24] and the evolution of the system topology after quench [25–29] having being actively investigated. In particular, experiments start to explore the band topology from quench dynamics [30,31]. By quenching across topological transition, a linking number can be obtained in the momentum-time domain to characterize the topology of the postquench band [30,32]. Unfortunately, to precisely detect the topology is more challenging. Chern invariants are detectable only in a few special cases, e.g., when the Chern band is flat [15], has inversion symmetry [18–20], or corresponds to a two-band model [30,32]. Precise detection is typically achieved only in deep topological regimes. Close to phase boundaries, measurement becomes increasingly imprecise due to a small topological gap and a nonideal condition such as thermal effects [20].

In this Letter, we explore a new dynamical approach to characterize a 2D quantum anomalous Hall (QAH) insulator. After the system Hamiltonian is quenched from a trivial to a topological parameter regime, a novel ring pattern of the spin dynamics emerges in momentum space during unitary evolution and uniquely corresponds to a nontrivial postquench topology. The configuration pattern, with the ring surrounding the Γ or the M point of the first Brillouin zone (FBZ), yields the Chern number of the postquench band.

Our scheme uncovers topology by quantum quench dynamics and exhibits several advantages. First, the ring structure arises during short-time unitary evolution and is thus insensitive to imperfect conditions such as thermal effects, which are relevant to longtime dynamics and to equilibrium dynamics. Second, unlike the linking number defined for 3D momentum-time space, the ring pattern is a 1D object, making the scheme simple and robust. Third, our experiment is the first clear evidence of so-called bulk-surface (bulk-ring in 2D) correspondence [33], which is universal for generic multiband systems for arbitrary dimensions. These advantages lead to a highly precise determination of the full topological phase diagram.

Quenching the 2D spin-orbit coupled Bose gas.—Our experiment is based on a QAH model [34] for 2D SO coupling [19,35] in a highly controllable Raman lattice [20,36]. The 2D SO coupling is induced by periodic Raman potentials along the x and y directions [Fig. 1(a)]. We define the $|1,-1\rangle$ ($|1,0\rangle$) state of ^{87}Rb as spin-up $|\uparrow\rangle$ (spin-down $|\downarrow\rangle$) [Fig. 1(b)]. The effective Hamiltonian reads

$$H = \frac{p^2}{2m} + V_{\text{latt}} + \frac{\delta}{2}\sigma_z + M_1(x,y)\sigma_x + M_2(x,y)\sigma_y, \qquad (1)$$

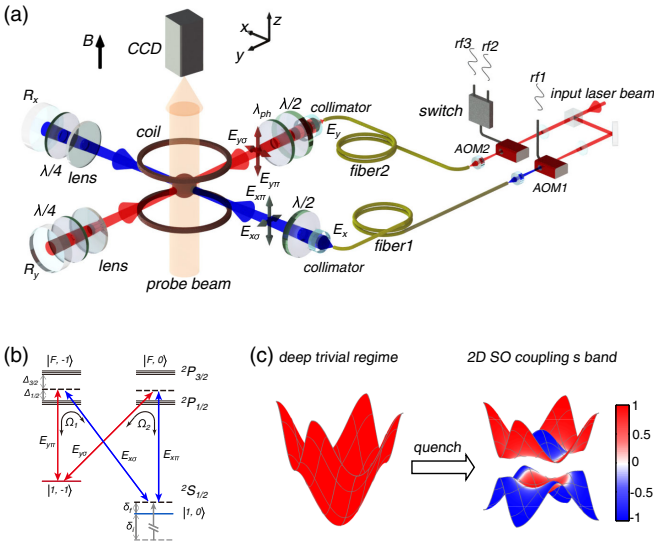

FIG. 1. (a) Experimental scheme. Two laser beams E_x and E_y are incident on the atoms and generate 2D lattice and Raman coupling. A bias magnetic field B is along the z direction. All wave plates ($\lambda/2$, $\lambda/4$ and λ_{ph}) are for realizing C_4-symmetric 2D SO coupling [20]. Laser-beam frequencies are controlled by AOM1 and AOM2, with phase-locked radio-frequency signaling rf1, rf2, and rf3. The switch is for quenching by switching rf2 and rf3 to change the two-photon detuning of the Raman couplings. (b) Level structure and Raman transitions. Raman coupling strengths Ω_1 and Ω_2 are induced by $(E_{x\sigma}, E_{y\pi})$ and $(E_{y\sigma}, E_{x\pi})$, respectively, and δ_i and δ_f represent two-photon detuning before and after quenching. (c) s-band structure before and after the quantum quench with the spin polarization of the equilibrium distribution presented.

where $V_{\text{latt}} = -V_0(\cos^2 k_0 x + \cos^2 k_0 y)$ is the 2D lattice potential with lattice depth V_0, δ is the two-photon Raman detuning, and $M_1 = \Omega_0 \cos k_0 x \sin k_0 y$ and $M_2 = \Omega_0 \cos k_0 y \sin k_0 x$ are Raman coupling lattices [20,36]. We focus on the symmetric case in which $M_{1,2}$ have the same amplitude Ω_0 and the 2D SO coupling is formed with a C_4 symmetry [20,36].

A gas of ^{87}Rb atoms is optically pumped into the $|\uparrow\rangle$ state and cooled to a temperature just above the Bose-Einstein condensate. Atoms are then adiabatically loaded into the 2D optical lattice in 100 ms to maintain thermal equilibrium. At this stage, the initial two-photon detuning is set at $\delta_i = -200E_r$. Thus, the Raman couplings M_1 and M_2 are effectively suppressed. The system is fully spin polarized in a topological trivial band.

Quench dynamics starts at time $t = 0$, when δ is switched from its initial value δ_i to a final near-resonant value δ_f within 200 ns, and nonzero M_1 and M_2 are introduced. The band structure thus switches from 2D lattice bands to 2D SO-coupling bands, shown in Fig. 1(c). This rapid quench projects the initial fully spin-polarized state onto superpositions of different eigenstates of the postquench Hamiltonian $H(\delta_f)$. This quench initiates a nonequilibrium evolution of Raman-induced Rabi oscillations between the $|\uparrow\rangle$ and $|\downarrow\rangle$ states governed by $H(\delta_f)$. Spin oscillation is quantified by the momentum-dependent spin polarization $P(\boldsymbol{q},t) = [(N_\uparrow - N_\downarrow)/(N_\uparrow + N_\downarrow)]$, where $N_\uparrow$ ($N_\downarrow$) denotes the number of atoms detected in the spin-up (-down) state at quasimomentum $\boldsymbol{q}$.

After the quench from δ_i to δ_f, we let the system evolve for a delay time t, and $P(\boldsymbol{q}, t)$ is then obtained by spin-resolved TOF imaging [37]. Measurements are repeated for various momenta $\boldsymbol{q}$ in the FBZ, and a sequence of times t are taken for each $\boldsymbol{q}$. Examples are shown in Fig. 2.

We now remark on the quench spin dynamics. For clarity, we focus on the lowest s band. All atoms are initialized in the spin-up state. Postquench spin dynamics is governed by two properties, namely, the Raman coupling terms $M_{1,2}$ and the local gap $\Delta(\boldsymbol{q})$ between the $|\uparrow\rangle$ and $|\downarrow\rangle$ bands at $\boldsymbol{q}$. The former controls the spin flip in the x-y plane, and the latter, defined for $H(\delta_f)$ by setting $M_{1,2} \to 0$ [37], serves as a momentum-dependent detuning for the Raman couplings. For momenta with $\Delta(\boldsymbol{q}) = 0$, coupling between the $|\uparrow\rangle$ and $|\downarrow\rangle$ bands is resonant, and the initial $|\uparrow\rangle$ state can be fully flipped to the $|\downarrow\rangle$ state during the unitary evolution.

Uncovering the topology: Dynamical ring pattern.—We first interpret the spin dynamics shown in Fig. 2(a), for which $\delta_f = 0$ and $(V_0, \Omega_0) = (4.0, 1.0)E_r$. Vanishing two-photon detuning δ_f implies that the postquench band at equilibrium is gapless and has two Dirac points at $\{X_{1,2}\} = \{(0,\pi), (\pi,0)\}$. Intriguingly, a straight-line pattern of spin-down components connecting the Dirac points emerges for short-time spin dynamics (< 2 ms), for which the spin

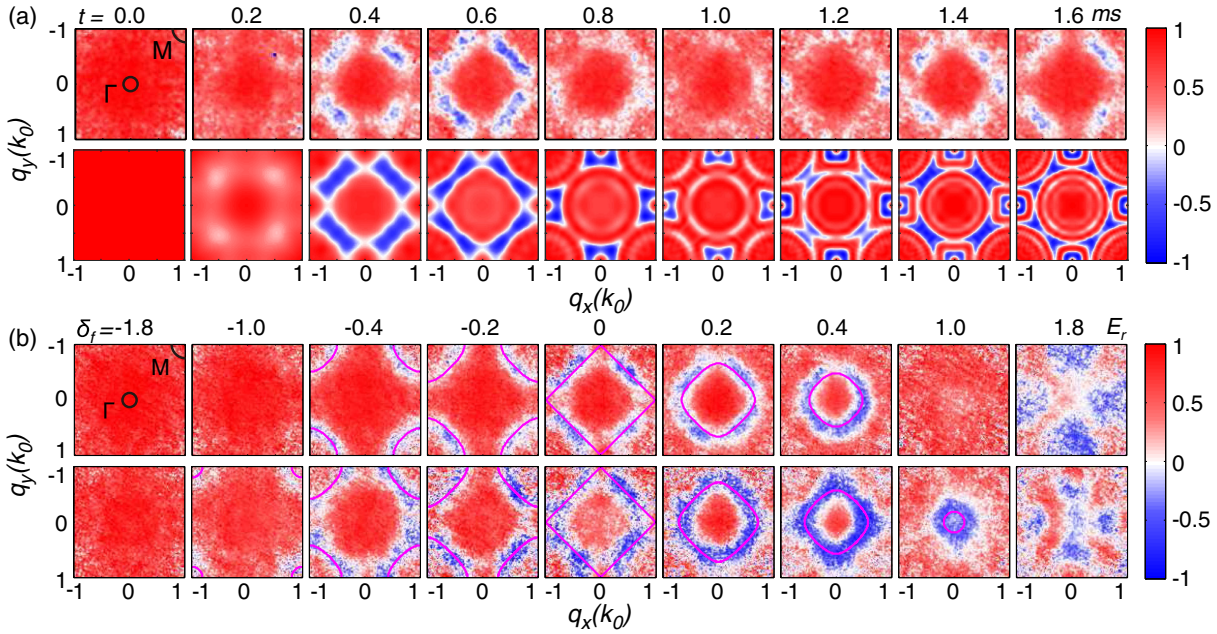

FIG. 2. Ring structure of spin polarization. (a) Evolution of $P(\boldsymbol{q}, t)$ in the FBZ from $t = 0$ to 1.6 ms, with parameters $(V_0, \Omega_0) = (4.0, 1.0)E_r$ and $\delta_f = 0$. The upper row is from experimental measurements, and the lower row is from theoretical calculations. (b) Spin polarization in the FBZ at fixed evolution time t versus δ_f. The upper row is for $(V_0, \Omega_0) = (4.0, 1.0)E_r$ and $t = 480$ μs, and the lower row is for $(V_0, \Omega_0) = (4.0, 2.0)E_r$ and $t = 320$ μs.

evolution is almost unitary, as decoherence and dissipation are much slower. Such a straight-line pattern highlights the momenta where the $|\uparrow\rangle$ and $|\downarrow\rangle$ bands of the Hamiltonian $H(\delta_f, M_{1,2} \to 0)$ cross with each other; i.e., $\Delta(\boldsymbol{q}) = 0$.

For small but nonzero two-photon detuning, we observe the emergence of a ring structure in the spin dynamics $P(\boldsymbol{q}, t)$. Figure 2(b) shows spin polarization patterns for a fixed evolution time as a function of δ_f. For $\delta_f = 0.2E_r$ and $0.4E_r$, spin polarization $P(\boldsymbol{q}, t)$ shows a ring pattern surrounding the Γ point, whereas for $\delta_f = -0.2E_r$ and $-0.4E_r$, $P(\boldsymbol{q}, t)$ shows arcs around the corners of the FBZ, representing a ring surrounding the M point. The straight-line pattern for $\delta_f = 0$ separates the $\delta_f > 0$ and the $\delta_f < 0$ regime, illustrating the phase transition between [19,20,34]. By comparison, at larger detuning (as $\delta_f = \pm 1.0E_r$ for $\Omega = 1.0E_r$, and $\delta_f = \pm 1.8E_r$ for $\Omega = 2.0E_r$), no dynamical ring pattern appears, implying that the topology of the postquench band is δ_f dependent. For $0 < |\delta_f| < \delta_c$, with δ_c as a critical value, the postquench band is topologically nontrivial with Chern number $\mathcal{C} = \mathrm{sgn}(\delta_f)$. For $|\delta_f| > \delta_c$, the topology is trivial. These results suggest that ring-pattern emergence signifies nontrivial topology of the system, and the ring pattern surrounding the Γ or M point provides additionally the sign of the Chern number for the postquench band. The "broken" ring connecting the gapless Dirac points measures the boundary, across which the Chern number varies between -1 and $+1$.

A theoretical explanation follows. Because of inversion and C_4 symmetry, band topology can be determined by the products $\Theta = \prod_{j=1}^{4} \mathrm{sgn}[S(\boldsymbol{\Lambda}_\mathbf{j})]$ of the lowest s-band Bloch states, where $S(\boldsymbol{\Lambda}_\mathbf{j})$ denotes the equilibrium spin polarization at the four symmetric momenta $\{\boldsymbol{\Lambda}_\mathbf{j}\} = \{\Gamma, M, X_{1,2}\}$ [18–20,34]. The value $\Theta = -1$ $(+1)$ corresponds to the topological (trivial) state [18]. Thus, the topological regime necessitates that one of the spin polarizations, $S(\Gamma)$ or $S(M)$, is the opposite of those of the other three. Accordingly, $S(\boldsymbol{q})$ must change its sign and pass through zero when it goes from the Γ (M) point to the other symmetry points. All of the momenta in the FBZ with $S(\boldsymbol{q}) = 0$ form a ring that coincides with the crossing between the spin-up and spin-down bands for $H(\delta_f, M_{1,2} \to 0)$. Such a ring is known as the band-inversion ring [33], across which the spin-up and spin-down bands are inverted (see the Supplemental Material [37] and Refs. [38–40] for details). The formation of this band-inversion ring corresponds to $\Delta(\boldsymbol{q}) = 0$ in the dynamical regime, leading to resonant oscillations between the spin-up and spin-down states. This oscillation creates the dynamical ring pattern in Fig. 2. Emergence of the dynamical ring pattern is thus a witness of nontrivial band topology.

We can further extract the Chern number of the postquench band from the ring pattern. As all atoms are initialized in the spin-up state with large detuning of minus sign, a small $\delta_f < 0$ implies that $S(\boldsymbol{\Lambda}_\mathbf{j})$ flips to spin-down for only one of the four symmetric momenta of the lowest band. From Fig. 2(b), we see emergence of the ring pattern surrounding the M point for the topological regime with $-\delta_c < \delta_f < 0$, indicating that the spin polarization of the lowest band at the M point must be negative $S(M) < 0$, whereas the other three are positive. Accordingly, the lowest-band Chern number can be determined directly with

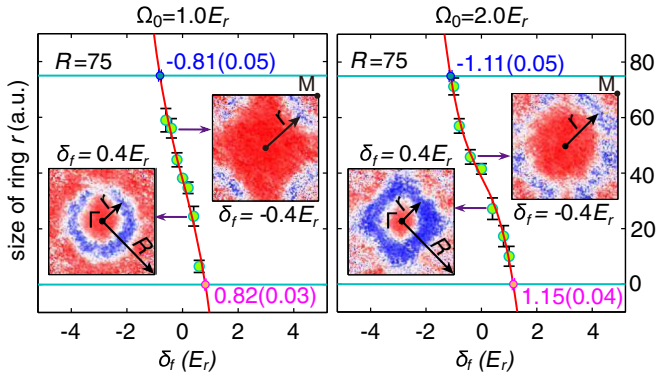

FIG. 3. Topological phase boundaries for $(V_0, \Omega_0) = (4.0, 1.0)E_r$ and $(4.0, 2.0)E_r$. The size r of the ring pattern (the insets) is measured as a function of δ_f, shown as the green circles with statistical error bars. The solid curves are the polynomial fitting results up to third order, giving the upper and the lower phase boundaries, marked as the cross points with $(r = 0)$ and $(r = R)$ lines, respectively.

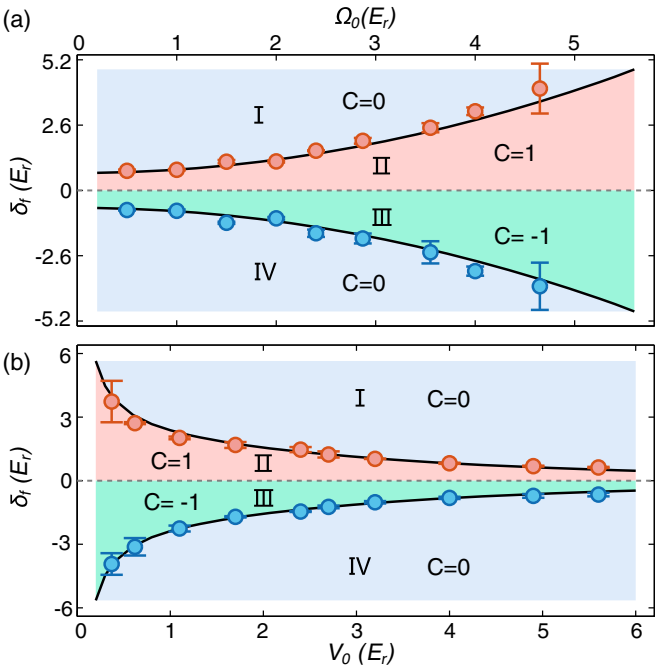

FIG. 4. Topological phase diagram for (a) $(\delta_f - \Omega_0)$ plane with $V_0 = 4.0E_r$, and (b) $(\delta_f - V_0)$ plane with $\Omega_0 = 1.0E_r$. The blue and red dots with statistical error bars are determined from the experiment, and the solid lines are from theoretical calculation with the same parameters. Areas I and IV are topological trivial areas with $\mathcal{C} = 0$, while areas II and III are topological nontrivial areas with $\mathcal{C} = 1$ and $\mathcal{C} = -1$, respectively.

$\mathcal{C} = [(\Theta - 1)/4] \sum_{j=1}^{4} \mathrm{sgn}[S(\mathbf{\Lambda_j})] = -1$ in this regime, with $\Theta = -1$ [18]. For a final detuning $0 < \delta_f < \delta_c$, the ring pattern encloses the Γ point, leading by similar analysis to $S(\Gamma) > 0$ and $S(X_{1,2}), S(M) < 0$, and hence $\mathcal{C} = +1$.

Precise determination of the topological phase diagram.—Spin dynamics is resonant only on the band-inversion rings, and we can determine the phase diagram of the band topology by measuring the size of the ring pattern as a function of δ_f. Experimental data for $(V_0, \Omega_0) = (4.0, 1.0)E_r$ and $(4.0, 2.0)E_r$ are shown in Fig. 3, in which the distance r between the Γ point and the ring is plotted versus the detuning δ_f. As δ_f is varied from 0 to δ_c^+, the size of the ring pattern shrinks and then disappears at the Γ point for $\delta_f = \delta_c^+$, giving the upper boundary of the topological zone. On the other side, as δ_f varies from 0 to δ_c^-, the distance r increases until the ring pattern disappears at the M point $(r = R)$ for $\delta_f = \delta_c^-$, giving the lower boundary. A polynomial fit up to third order gives the phase boundaries as $(\delta_c^+, \delta_c^-) = (0.82 \pm 0.03, -0.81 \pm 0.05)E_r$ and $(1.15 \pm 0.04, -1.11 \pm 0.05)E_r$ for $(V_0, \Omega_0) = (4.0, 1.0)E_r$ and $(4.0, 2.0)E_r$, respectively.

With these measurements, we obtain the full topological phase diagram, shown in Figs. 4(a) and 4(b). Remarkably, the estimated phase boundary is highly consistent with the theoretical calculation over the entire parameter range. The lattice depth $V_0 = 4.0E_r$ is very small, so higher-band effects can become relevant for longer-time dynamics and at equilibrium. The high precision, achieved by the present dynamical approach, demonstrates its great advantage over previous approaches at equilibrium [19,20], where the measured topological phase diagram deviates from the theoretical prediction [36].

Long-time dynamics.—Beyond the emergent ring structure evident during the initial unitary evolution, spin polarization $P(\boldsymbol{q}, t)$ displays intriguing long-time dynamics (for details, see the Supplemental Material [37] and Refs. [41,42]). Spin polarization is oscillatory with $\boldsymbol{q}$-dependent frequencies $\omega(\boldsymbol{q})$ and eventually relaxes to its equilibrium value. Measuring $\omega(\boldsymbol{q})$ throughout the FBZ allows us to reconstruct the band structure of the Hamiltonian $H(\delta_f)$ [37]. Further, $P(\boldsymbol{q}, t \gg 0)$ would change (keep) its sign for a $\boldsymbol{q}$ outside (inside) the ring, directly revealing the topology of the postquench Hamiltonian.

Conclusion and discussion.—In this Letter, we show that quantum quench dynamics provides a robust and powerful method to uncover topology of cold-atom systems. A topological (trivial) phase of a 2D system is simply identified from emergence (absence) of a 1D ring structure, and the Chern number is read out according to whether the ring encloses the Γ or the M points. Measuring the ring size, versus the two-photon detuning δ_f, leads to a highly precise determination of the full topological phase diagram. Our method is insensitive to imperfect conditions such as thermal effects and, further, remains valid in the presence of weak interactions as long as the band-inversion ring is well defined.

By inferring topology of a 2D system from a 1D ring, we demonstrate that a higher-dimensional topological system can be characterized by a lower-dimensional invariant [38–40]. This approach was proposed to generic topological phases and yield a fundamental dynamical classification theory of topological quantum states [33]. Our work

establishes an insightful and powerful approach to explore novel topological quantum states with nonequilibrium dynamics.

We acknowledge insightful discussions with Ting-Fung Jeffrey Poon, Long Zhang, and Hui Zhai. This work was supported by the National Key R&D Program of China (Grants No. 2016YFA0301601 and No. 2016YFA0301604), the National Natural Science Foundation of China (Grants No. 11674301, No. 11761161003, and No. 11625522), and the Thousand-Young-Talent Program of China. W.-W. Z. is supported by the Australian Research Council (ARC) via Centre of Excellence in Engineered Quantum Systems (EQuS) Project No. CE110001013. J. S. acknowledges support from the European Research Council, ERC-AdG "QuantumRelax".

*xiongjunliu@pku.edu.cn
†shuai@ustc.edu.cn
‡pan@ustc.edu.cn

[1] K. von Klitzing, G. Dorda, and M. Pepper, Phys. Rev. Lett. **45**, 494 (1980).
[2] D. C. Tsui, H. L. Stormer, and A. C. Gossard, Phys. Rev. Lett. **48**, 1559 (1982).
[3] X.-G. Wen, Int. J. Mod. Phys. B **04**, 239 (1990).
[4] M. Z. Hasan and C. L. Kane, Rev. Mod. Phys. **82**, 3045 (2010).
[5] X. L. Qi and S. C. Zhang, Rev. Mod. Phys. **83**, 1057 (2011).
[6] M. König, S. Wiedmann, C. Brune, A. Roth, H. Buhmann, L. W. Molenkamp, X.-L. Qi, and S.-C. Zhang, Science **318**, 766 (2007).
[7] D. Hsieh, D. Qian, L. Wray, Y. Xia, Y. S. Hor, R. J. Cava, and M. Z. Hasan, Nature (London) **452**, 970 (2008).
[8] Y. Xia, D. Qian, D. Hsieh, L. Wray, A. Pal, H. Lin, A. Bansil, D. Grauer, Y. S. Hor, R. J. Cava, and M. Z. Hasan, Nat. Phys. **5**, 398 (2009).
[9] C.-Z. Chang *et al.*, Science **340**, 167 (2013).
[10] F. Wilczek, Nat. Phys. **5**, 614 (2009).
[11] J. Alicea, Rep. Prog. Phys. **75**, 076501 (2012).
[12] M. Franz, Nat. Nanotechnol. **8**, 149 (2013).
[13] S. R. Elliott and M. Franz, Rev. Mod. Phys. **87**, 137 (2015).
[14] M. Atala, M. Aidelsburger, J. T. Barreiro, D. Abanin, T. Kitagawa, E. Demler, and I. Bloch, Nat. Phys. **9**, 795 (2013).
[15] G. Jotzu, M. Messer, R. Desbuquois, M. Lebrat, T. Uehlinger, D. Greif, and T. Esslinger, Nature (London) **515**, 237 (2014).
[16] M. Aidelsburger, M. Lohse, C. Schweizer, M. Atala, J. T. Barreiro, S. Nascimbène, N. R. Cooper, I. Bloch, and N. Goldman, Nat. Phys. **11**, 162 (2015).
[17] N. Fläschner, B. S. Rem, M. Tarnowski, D. Vogel, D. S. Luhmann, K. Sengstock, and C. Weitenberg, Science **352**, 1091 (2016).
[18] X.-J. Liu, K. T. Law, T. K. Ng, and P. A. Lee, Phys. Rev. Lett. **111**, 120402 (2013).
[19] Z. Wu, L. Zhang, W. Sun, X.-T. Xu, B.-Z. Wang, S.-C. Ji, Y. Deng, S. Chen, X.-J. Liu, and J.-W. Pan, Science **354**, 83 (2016).
[20] W. Sun, B.-Z. Wang, X.-T. Xu, C.-R. Yi, L. Zhang, Z. Wu, Y. Deng, X.-J. Liu, S. Chen, and J.-W. Pan, Phys. Rev. Lett. **121**, 150401 (2018).
[21] J. C. Budich and M. Heyl, Phys. Rev. B **93**, 085416 (2016).
[22] P. Jurcevic, H. Shen, P. Hauke, C. Maier, T. Brydges, C. Hempel, B. P. Lanyon, M. Heyl, R. Blatt, and C. F. Roos, Phys. Rev. Lett. **119**, 080501 (2017).
[23] N. Fläschner, D. Vogel, M. Tarnowski, B. S. Rem, D. S. Luhmann, M. Heyl, J. C. Budich, L. Mathey, K. Sengstock, and C. Weitenberg, Nat. Phys. **14**, 265 (2018).
[24] M. Heyl, Rep. Prog. Phys. **81**, 054001 (2018).
[25] L. D'Alessio and M. Rigol, Nat. Commun. **6**, 8336 (2015).
[26] M. D. Caio, N. R. Cooper, and M. J. Bhaseen, Phys. Rev. Lett. **115**, 236403 (2015).
[27] Y. Hu, P. Zoller, and J. C. Budich, Phys. Rev. Lett. **117**, 126803 (2016).
[28] F. N. Ünal, E. J. Mueller, and M. Ö. Oktel, Phys. Rev. A **94**, 053604 (2016).
[29] J. H. Wilson, J. C. W. Song, and G. Refael, Phys. Rev. Lett. **117**, 235302 (2016).
[30] M. Tarnowski, F. N. Ünal, N. Fläschner, B. S. Rem, A. Eckardt, K. Sengstock, and C. Weitenberg, arXiv:1709.01046.
[31] B. Song, L. Zhang, C. He, T. F. J. Poon, E. Hajiyev, S. Zhang, X.-J. Liu, and G.-B. Jo, Sci. Adv. **4**, eaao4748 (2018).
[32] C. Wang, P. Zhang, X. Chen, J. Yu, and H. Zhai, Phys. Rev. Lett. **118**, 185701 (2017).
[33] L. Zhang, L. Zhang, S. Niu, and X.-J. Liu, Sci. bull. **63**, 1385 (2018).
[34] X.-J. Liu, K. T. Law, and T. K. Ng, Phys. Rev. Lett. **112**, 086401 (2014); **113**, 059901 (2014).
[35] L. Zhang and X.-J. Liu, in *Synthetic Spin-Orbit Coupling in Cold Atoms*, edited by W. Zang, W. Yi, and C. A. R. Sá Melo (World Scientific, Singapore, 2018), pp. 1–87.
[36] B.-Z. Wang, Y.-H. Lu, W. Sun, S. Chen, Y. Deng, and X.-J. Liu, Phys. Rev. A **97**, 011605(R) (2018).
[37] See Supplemental Material at http://link.aps.org/supplemental/10.1103/PhysRevLett.121.250403 for details.
[38] C. Chan, L. Zhang, T. F. J. Poon, Y.-P. He, Y.-Q. Wang, and X.-J. Liu, Phys. Rev. Lett. **119**, 047001 (2017).
[39] T. F. J. Poon and X.-J. Liu, Phys. Rev. B **97**, 020501(R) (2018).
[40] W.-W. Zhang, B. C. Sanders, S. Apers, S. K. Goyal, and D. L. Feder, Phys. Rev. Lett. **119**, 197401 (2017).
[41] S. Matsuo, T. Fujii, N. Kosugi, and N. Hatakenaka, J. Phys. Conf. Ser. **150**, 022056 (2009).
[42] F. M. Izrailev and A. Castañeda-Mendoza, Phys. Lett. A **350**, 355 (2006).